The Cryosphere Discuss., https://doi.org/10.5194/tc-2018-223
Manuscript under review for journal The Cryosphere
Discussion started: 12 November 2018

The Cryosphere Discussions
Open Access
EGU

Estimating the snow depth, the snow-ice interface temperature, and the effective temperature of Arctic sea ice using Advanced Microwave Scanning Radiometer 2 and Ice Mass Balance buoys data

Lise Kilic[1], Rasmus Tage Tonboe[2], Catherine Prigent[1], and Georg Heygster[3]

[1]Sorbonne Université, Observatoire de Paris, Université PSL, CNRS, LERMA, Paris, France
[2]Danish Meteorological Institute, Copenhagen, Denmark
[3]Institute of Environmental Physics, University of Bremen, Bremen, Germany

Correspondence: Lise Kilic (lise.kilic@obspm.fr)

Abstract. Mapping Sea Ice Concentration (SIC) and understanding sea ice properties and variability is important especially today with the recent Arctic sea ice decline. Moreover, accurate estimation of the sea ice effective temperature (T_{eff}) at 50 GHz is needed for atmospheric sounding applications over sea ice and for noise reduction in SIC estimates. At low microwave frequencies, the sensitivity to atmosphere is low, and it is possible to derive sea ice parameters due to the penetration of microwaves in the snow and ice layers. In this study, we propose simple algorithms to derive the snow depth, the snow-ice interface temperature ($T_{Snow-Ice}$) and the T_{eff} of Arctic sea ice from microwave brightness temperatures (TBs). This is achieved using the Round Robin Data Package of the ESA sea ice CCI project, which contains TBs from the Advanced Microwave Scanning Radiometer 2 (AMSR2) collocated with measurements from Ice Mass Balance (IMB) buoys and the NASA Operation Ice Bridge (OIB) airborne campaigns over the Arctic sea ice. The snow depth over sea ice is estimated with an error of ∼6 cm using a multilinear regression with the TBs at 6V, 18V, and 36V. The $T_{Snow-Ice}$ is retrieved using a linear regression as a function of the snow depth and the TBs at 10V or 6V. The Root Mean Square Errors (RMSEs) obtained are 1.69 and 1.95 K respectively, with the 10V and 6V TBs. The T_{eff} at microwave frequencies between 6 and 89 GHz is expressed as a function of $T_{Snow-Ice}$ using data from a thermodynamical model combined with the Microwave Emission Model of Layered Snow-packs. T_{effs} are estimated from the $T_{Snow-Ice}$ with a RMSE of less than 1 K.

1 Introduction

In situ observations of the variables controling the sea ice energy and momentum balance in polar regions are scarce. One way to overcome this observational gap is to use satellites for measuring sea ice properties. The objective of this study is to estimate key sea ice variables from satellite remote sensing to improve Sea Ice Concentration (SIC) mapping and polar atmospheric sounding applications.

Sea ice dynamics and thermodynamics is controlled by the regional heat budget (Maykut and Untersteiner, 1971). In general, sea ice is covered by snow, which can reach a mean thickness of up to ∼50 cm in the Arctic (Sato and Inoue, 2018). Snow on sea ice strongly affects the sea ice energy and radiation balance, with its high insulation and reflectivity of solar radiation. Snow

The Cryosphere Discuss., https://doi.org/10.5194/tc-2018-223
Manuscript under review for journal The Cryosphere
Discussion started: 12 November 2018

is a poor conductor of heat: it insulates the sea-ice and reduces the winter ice growth. In summer, its high albedo reduced the sea-ice melting rate. Sato and Inoue (2018) suggest that the recent sea ice growth has been effectively limited by the increase in snow depth on thin ice during winter. Current sea ice models include snow schemes (e.g., Lecomte et al. (2011)), with the snow depth and temperature gradient in the snow pack modulating the sea ice growth and melt. Improved estimates of Snow Depth (SD), as well as Snow-Ice interface Temperature ($T_{Snow-Ice}$) from satellite observations would provide valuable information on the vertical thermodynamics in the snow and ice, to improve current sea ice models and therefore the prediction of sea ice growth.

Here we propose a simple algorithm to retrieve the snow depth and the $T_{Snow-Ice}$ from passive microwave observations from the Advance Microwave Scanning Radiometer 2 (AMSR2), based on a large dataset of collocated *in situ* and satellite observations. An extensive Round Robin Data Package (RRDP) has been developed during the European Space Agency (ESA) sea ice Climate Change Initiative (CCI) project (http://www.seaice.dk/ecv2/rrdb-v1.1/). It contains *in situ* data from the Ice Mass Balance (IMB) buoys, and the Operation Ice Bridge (OIB) airborne campaigns collocated with AMSR2 brightness temperature measurements between 6 and 89 GHz. Algorithms already exist to retrieve the snow depth from microwave observations. Markus and Cavalieri (1998) and Comiso et al. (2003) use the spectral gradient ratio of the 18.7 and 37 GHz in vertical polarization to deduce the snow depth over sea ice. This method has been developed for dry snow in Antarctica. With the help of the RRDP, we will revisit the methodology for the Arctic region. Tonboe et al. (2011) showed from radiative transfer simulations that there is a high linear correlation between the $T_{Snow-Ice}$ and the passive microwave observations at 6 GHz. Preliminary results from (Grönfeldt, 2015) evidenced the possibility to derive the temperature of sea ice from passive microwave observations using simple regression models. This work will be extended here.

Passive microwave satellite observations between 50 and 60 GHz are extensively used to provide the atmospheric temperature profiles in Numerical Weather Prediction (NWP) centers, with instruments such as the Advanced Microwave Sounding Unit-A (AMSU-A) or the Advanced Technology Microwave Sounder (ATMS). For an accurate estimation of the temperature profile in the lower atmosphere, quantifying the surface contribution is required. The surface contribution depends on frequency and it is the product of the surface emissivity and the surface effective Temperature (T_{eff}). T_{eff} is defined as the integrated temperature over a layer corresponding to the penetration depth of the given frequency: the larger the wavelength, the deeper the penetration in the medium. The problem is particularly complicated over sea ice, due to its large spatial and temporal variability and the interaction between the radiation and the medium (English, 2008; Tonboe et al., 2013; Wang et al., 2017). The layering and the vertical structure in the snowpack, as well as the scattering from snow grains and voids, are affecting the microwave emission processes (Mathew et al., 2008; Rosenkranz and Mätzler, 2008; Harlow, 2009, 2011; Tonboe, 2010; Tonboe et al., 2011). The relationship between T_{eff} and the physical temperature profile is complicated, especially at microwave frequencies $\geq$18 GHz, but it has been shown that from 6 to 50 GHz, there is a high correlation between the T_{eff} and the $T_{Snow-Ice}$ (Tonboe et al., 2011). With $T_{Snow-Ice}$ estimated from the AMSR2 observations, we will deduce the sea ice T_{eff} at AMSR2 frequencies between 6 and 89 GHz, using linear regression.

Section 2 describes the dataset and the methodology used in this study. The snow depth retrieval is presented in Section 3. Section 4 reports on the $T_{Snow-Ice}$ retrieval. Finally, microwave sea ice T_{eff} at 50 GHz is derived, for application to

The Cryosphere Discuss., https://doi.org/10.5194/tc-2018-223
Manuscript under review for journal The Cryosphere
Discussion started: 12 November 2018

temperature atmospheric sounding (section 5). Secion 6 discuss the snow depth and the $T_{Snow-Ice}$ retrieval results over a winter over the Arctic. Section 7 concludes this study.

2 Materials and Methods

2.1 The database of collocated satellite observations and in situ measurements

The RRDP from the ESA sea ice CCI project is a dataset openly available. It contains an extensive collection of collocated satellite microwave radiometer data with *in situ* buoy or airborne campaign measurements and other geophysical parameters, with relevance for computing and understanding the variability of the microwave observations over sea ice. It covers areas with 0% and 100% of SIC and different sea ice types (thin ice, first-year ice, multiyear ice), for all seasons including summer melt. In our study, we will focus on Arctic sea ice during winter in regions with 100% sea ice cover. Two different dataset from the RRDP are used: AMSR2 brightness temperatures (TBs) collocated with IMB buoy measurements, and AMSR2 TBs collocated with OIB airborne campaign measurements.

AMSR2 is a passive microwave radiometer on board the JAXA GCOM-W1 satellite (launch on May 18, 2012). AMSR2 has 14 channels at 6.9, 7.3, 10.65, 18.7, 23.8, 36.5 and 89 GHz for both vertical and horizontal polarizations and it observes at 55° of incidence angle. In the RRDP, the spatial resolution of each channel is resampled to the 6.9 GHz resolution (32×62 km) before collocation with buoy or airborne campaign measurements (RRDP report, Pedersen and Saldo (2016)).

IMB buoys are installed by the Cold Regions Research and Engineering Laboratory (CRREL) to measure the ice mass balance of the Arctic sea ice cover. Buoy components include acoustic sounders and a string of thermistors. The thermistor string is extending from the air, through the snow cover and sea ice, into the water with the temperature sensors located every 10 cm along the string. It measures the physical temperature with an accuracy of 0.1 K. The acoustic sounder measures the position of snow and ice surfaces (i.e., the snow depth) with a precision of 5 mm. The buoys also include instruments to measure air temperature, barometric air pressure and GPS geographical position (Perovich et al., 2017). Several IMB buoys are deployed by the CRREL at different locations and times during the year. We only use Arctic buoy data recorded during winter (December 1^{st} to April 1^{st}) to avoid cases where ice has started to melt. A summary of buoys information corresponding to these criteria is given in Table 1 and the IMB buoy locations are shown in Figure 1. IMB buoy measurements collocated with AMSR2 TBs used in this study totalize 2845 observations.

For snow depth retrieval, we also used data from the OIB airborne campaign. The NASA OIB project has collected ice and snow depth data in the Arctic during annual flight campaigns (March-May) since 2009. The data are especially valuable in this context since they contain snow depth information from the snow radar onboard the aircraft, not only from single points, but continuously along the flight path. In the RRDP, the snow depth data from OIB radar are averaged into 50 km sections to be collocated with AMSR2 observations. For our study we use the OIB data from the 2013 campaign. It totalizes 408 observations over 8 days in March and April. Figure 1 summarizes the location of IMB buoys and OIB campaigns over the Arctic ocean.

It is important to note that there are discrepancies due to the scale, when comparing point measurements from buoys with the spatially averaged data from satellites or aircrafts (Dybkjær et al., 2012). The buoy data are neither interpolated or smoothed

The Cryosphere Discuss., https://doi.org/10.5194/tc-2018-223
Manuscript under review for journal The Cryosphere
Discussion started: 12 November 2018

Table 1. List of the IMB buoys used in this study.

Buoy ID	Duration of measurements during winter (dd/mm/yy)	Deployment location	Position on December 1st (lat; lon)	Mean snow depth (cm)	Mean ice thickness (cm)
2012G	01/12/12 - 06/02/13	Central Arctic	(85,79°; -134,88°)	34.1	162.8
2012H	01/12/12 - 06/02/13	Beaufort Sea	(80,39°; -129,23°)	23.2	173.3
2012J	01/12/12 - 06/02/13	Laptev Sea	(82,87°; 139,09°)	25.5	100.3
2012L	01/12/12 - 06/02/13	Beaufort Sea	(80,36°; -138,55°)	8.5	330.1
2013F	01/12/13 - 31/03/14	Beaufort Sea	(76,15°; -146,27°)	50.3	145.7
2013G	01/12/13 - 31/03/14	Beaufort Sea	(75,84°; -151,46°)	21.3	249.4
2014F	01/12/14 - 11/03/15	Beaufort Sea	(76,32°; -143,10°)	16.1	151.8
2014I	01/12/14 - 12/03/15	Beaufort Sea	(78,52°; -148,70°)	22.6	155.3

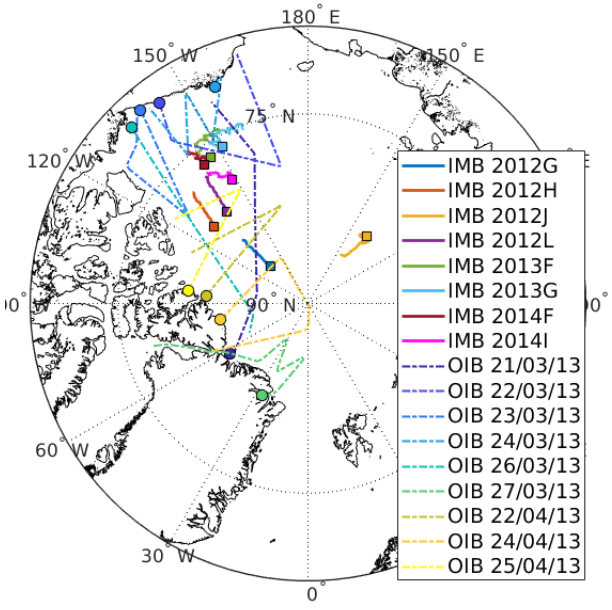

Figure 1. IMB buoys and OIB flight locations over Arctic sea ice. Squares indicate the position of IMB buoys on December 1st and circles indicate the starting points of OIB campaigns.

in time. E.g., in terms of surface air temperatures measured at adjacent buoys and ice stations there are about 1 K to 4 K differences per 100 km (Lindsay et al., 1994).

The Cryosphere Discuss., https://doi.org/10.5194/tc-2018-223
Manuscript under review for journal The Cryosphere
Discussion started: 12 November 2018

2.2 The database of simulated effective temperature and brightness temperature from sea ice properties

For estimation of the T_{eff}, we use a microwave emission model and a thermodynamical model to relate physical snow and ice properties to TBs and T_{effs} of sea ice. The model used here is a sea ice version of the Microwave Emission Model of Layered Snowpacks (MEMLS) (Wiesmann and Mätzler, 1999) described in Mätzler (2006). The simulations were part of an earlier version of the RRDP and the simulation methodology is described in Tonboe (2010).

2.3 Methodology

In this study, we propose simple algorithms, using multilinear regressions, to derive the snow depth, the $T_{Snow-Ice}$, and the T_{eff} of sea ice from AMSR2 TBs.

The measurements from the IMB buoys 2012G, 2012H, 2012J, and 2012L, collocated with AMSR2 TBs, are used as the training dataset for the different regressions to retrieve snow depth and $T_{Snow-Ice}$. These buoys have been selected because they are located in different regions across the Arctic and show a large range of snow depths. The measurements from IMB buoys 2013F, 2013G, 2014F and 2014I which are all located in the Beaufort sea are used as the testing dataset.

First, the IMB snow depth is expressed as a function of the AMSR2 TBs using a multilinear regression. The OIB data are used for the forward selection and the IMB buoy training dataset is used to perform the regression. Second, the $T_{Snow-Ice}$ is expressed as a function of TBs and snow depth, using linear regressions. An automated method to detect the position of the snow-ice interface on the vertical temperature profile measured by the IMB buoy thermistor string is developed (Section 4.1). Then, the IMB buoy training dataset is used to perform the regressions. For this part there are two consecutive regressions: the first one is done between the centered (the average was subtracted) $T_{Snow-Ice}$ and TBs ; the second one is done between the $T_{Snow-Ice}$ corrected for the TB dependence and the snow depth. Third, the sea ice T_{eff} at different microwave frequencies is expressed as a function of the $T_{Snow-Ice}$. This final step is using the simulations from a thermodynamical model and MEMLS to derive linear regression equations for the T_{eff} at frequencies between 6 and 89 GHz. The T_{eff} at 50 GHz is the one of interest for atmospheric sounding applications.

3 Snow depth estimation

3.1 Multilinear regression to retrieve the snow depth

A forward selection method is used to choose the best AMSR2 channels to retrieve snow depth. It is a statistical method to determine the best predictor combinations (here, AMSR2 TBs) to retrieve a variable (here, snow depth). Our training dataset for this forward selection is the OIB snow depth from the 2013 campaign included in the RRDP. OIB data are chosen for forward selection because the data cover a large area with a wide range of snow depths. In addition, the scale of the averaged OIB data is closer to satellite footprint than buoy measurements, increasing the consistency with the satellite observations. Forward selection tests have also been done with the IMB buoy training dataset but the results were not satisfying. We find

The Cryosphere Discuss., https://doi.org/10.5194/tc-2018-223
Manuscript under review for journal The Cryosphere
Discussion started: 12 November 2018

that the best channel combination for snow depth retrieval is the combination of the 3 channels at 6.9, 18.7, and 36.5 GHz in vertical polarization (6V, 18V, and 36V).

Then, a multilinear regression is conducted using the training dataset (IMB buoys G, H, J, L in 2012 collocated with AMSR2 TBs). The snow depth is given as a linear combination of the TBs at 6V, 18V, and 36V :

$$SD = 1.7701 + 0.0175 \cdot TB_{6V} - 0.0280 \cdot TB_{18V} + 0.0041 \cdot TB_{36V}, \quad (1)$$

with SD the snow depth expressed in m and TB in K. This model was trained with snow depths between 5 and 40 cm.

The forward selection has been also tested constraining the number of predictors to 2 and 4. The combinations obtained are: 18V and 36V for 2 channels, and 6V, 18V, 36V, and 89V for 4 channels. Then, the multilinear regression has been performed using these combinations of 2 or 4 channels. The results show that the 3 channel combination is the best (see results in Table 2), in terms of RMSE and correlation, comparing to the 2 or 4 channel combination (Comparing with IMB buoys measurements except 2013F buoy, RMSE=4.85 cm and R=0.68 using 2 channels, and RMSE=12.19 cm and R=0.52 using 4 channels. Comparing with OIB data, RMSE=8.04 cm, R=0.67 using 2 channels and RMSE=7.8 cm, R=0.87 using 4 channels).

3.2 Results of the snow depth retrieval

Figure 2 shows the comparison between the observed snow depth measured by the acoustic sounder of IMB buoys, the regressed snow depth computed from AMSR2 TBs with equation 1, and the snow depth estimate from Markus and Cavalieri (1998). The RMSE between the IMB buoys snow depth observations and our snow depth regression is 10.6 cm and the correlation coefficient is 0.65, using all the IMB buoys. For the Markus and Cavalieri (1998) snow depth, the RMSE is 15.7 cm and the correlation coefficient is 0.53. The snow depth estimation of Markus and Cavalieri (1998) fits well the snow depth from the buoy 2013F compared to our regression, but overestimates the snow depth of the buoy 2013G, 2014F, and 2014I by about 15 cm. Therefore, our snow depth regression is more appropriate for these buoy measurements except for the buoy 2013F.

The buoy 2013F observes a large snow depth ($>$ 40 cm) which is outside the bounds of our snow depth model. Tests are conducted to improve the estimation, including the 2013F buoy in the training dataset, with equal numbers of observations for different range of snow depths: it does not improve the results. The Markus and Cavalieri (1998) model and our model obtained the same snow depth estimation between buoys 2013G and 2013F. It is consistent because these buoys are spatialy very close. Therefore, we suspect that the 2013F buoy is located on a ridge or hummock where the local snow depth is large but not detectable at the satellite footprint scale. Without including the buoy 2013F in the computation, the RMSE for our snow depth model is 5.1 cm and the correlation coefficient is 0.77.

We also compare the snow depth retrievals with the measurements of the 2013 OIB campaigns (see Figure 3). For our snow depth regression (Eq. 1) and Markus and Cavalieri (1998) estimate, the RMSEs are 6.26 cm and 7.25 cm, respectively, and the correlation coefficients are both 0.87. All the results are summarized in Table 2. Note that the uncertainties on OIB data for the 2013 campaigns are between 2 cm and 22 cm with a mean standard deviation of 11 cm. Spatial scales are different when comparing satellite measurements or airborne campaign measurements (which have an extended footprint) with buoy

The Cryosphere Discuss., https://doi.org/10.5194/tc-2018-223
Manuscript under review for journal The Cryosphere
Discussion started: 12 November 2018

Table 2. Snow depth retrieval scores

Data and retrieval method	Correlation	RMSE (cm)
IMB buoys		
Our regression (Eq. 1)	0.65	10.6
Markus and Cavalieri (1998)	0.53	15.7
IMB buoys without 2013F		
Our regression (Eq. 1)	0.77	5.1
OIB campaigns (2013)		
Our regression (Eq. 1)	0.87	6.26
Markus and Cavalieri (1998)	0.87	7.25

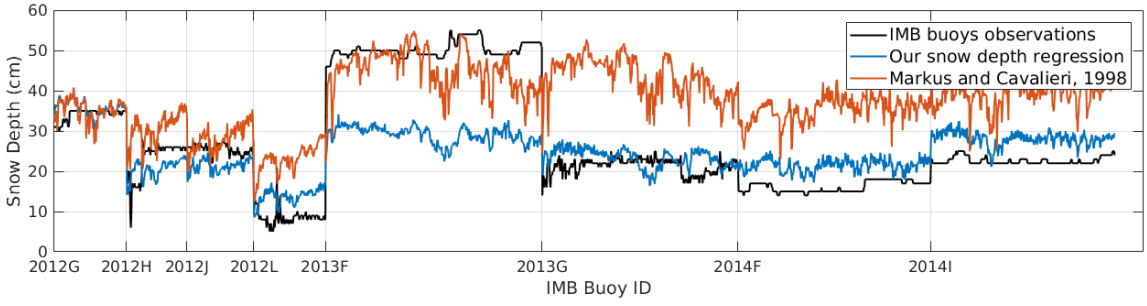

Figure 2. Time series of the comparison between snow depths from IMB buoy observations, our multilinear regression (Eq. 1), and the estimate of Markus and Cavalieri (1998). The begin of the measurements with a new IMB buoy is indicated on the x-axis.

measurements. Discrepancies can appear due to the spatial variability of the snow depth. It can explain that the correlation is higher when comparing snow depth estimated from AMSR2 TBs with the snow depth observed from OIB radar.

4 Snow-ice interface temperature estimation

4.1 Automatic interface position detection

During winter the air temperature is very cold (-30°C) meaning that the snow surface temperature is cold compared to ice and water temperatures. Through sea ice, the temperature profile is nearly piecewise linear and temperature increases with depth (see Figure 4). In the air, the temperature gradient is small because of turbulent mixing. In the snow, the temperature gradient is highest (∼35 K/m) due to the thermal properties of snow. Therefore, air-snow and snow-ice interface positions can be detected by changes in the temperature gradient. At the snow-air interface the second derivative of the temperature profile reaches a

The Cryosphere Discuss., https://doi.org/10.5194/tc-2018-223
Manuscript under review for journal The Cryosphere
Discussion started: 12 November 2018

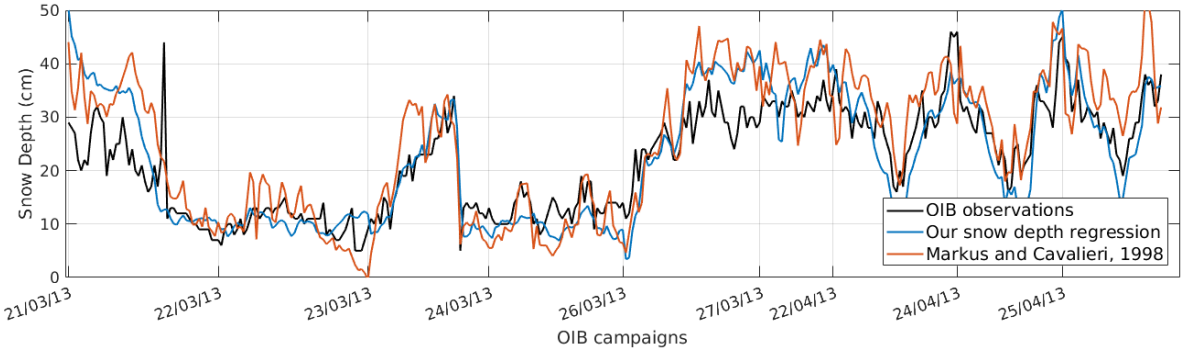

Figure 3. Time series of the comparison between snow depths from OIB observations, our multilinear regression (Eq. 1), and the estimate of Markus and Cavalieri (1998). The begin of the measurements with a new OIB campaign is indicated on the x-axis.

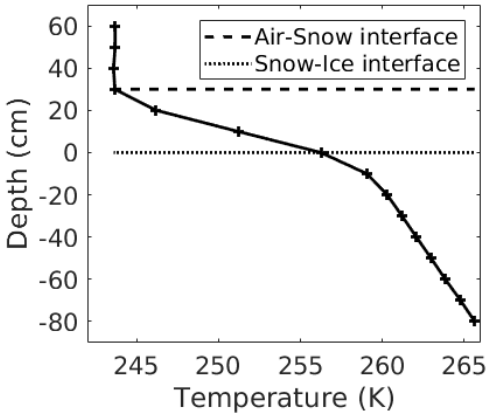

Figure 4. Averaged temperature profile (From December to February) measured by the IMB buoy 2012G, with air-snow and snow-ice interface levels detected with our automated method.

maximum. At the snow-ice interface, the temperature gradient being lower in the ice than in the snow, the second derivative of the temperature profile reaches a minimum. Using these properties of the sea ice temperature profile, an automated method is implemented to detect the air-snow and the snow-ice interface positions in the temperature profile measured by the buoy thermistor string.

Figure 4 shows an averaged temperature profile through sea ice during winter, with the air-snow and snow-ice interface positions detected with our automated method. This method performs best during winter when the air is cold. It may not be applicable if the snow depth is lower than the vertical resolution of the thermistor string (10 cm), or if sea ice start to melt and the temperature profile develops gradually toward an isothermal state.

The Cryosphere Discuss., https://doi.org/10.5194/tc-2018-223
Manuscript under review for journal The Cryosphere
Discussion started: 12 November 2018

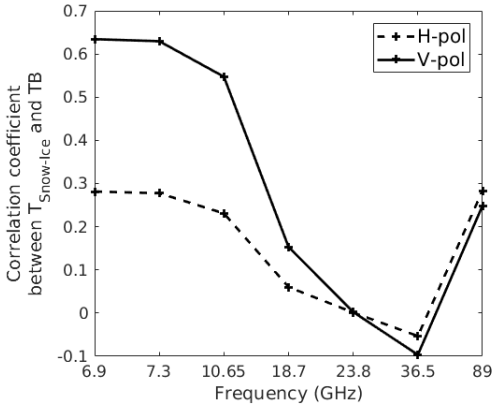

Figure 5. Correlation coefficient between the $T_{Snow-Ice}$ from IMB buoys and the AMSR2 TBs.

4.2 Correlation between the brightness temperature and the snow-ice interface temperature

During winter, the vertical position of the snow-ice interface, with respect to the buoy thermistor string, is fixed. The thermistor string is frozen into the ice which means that the thermistor at the snow-ice interface will stay at that interface unless there is surface melt or snow ice formation and this rarely happens during winter. For each IMB buoy, the snow-ice interface is detected with our automated method described in section 4.1.

We use a correlation analysis to select the TBs at different frequencies describing the variability of the $T_{Snow-Ice}$. Figure 5 shows the correlation coefficient between $T_{Snow-Ice}$ and AMSR2 TBs computed using the data from all IMB buoys (Table 1). The 89 GHz TBs are highly correlated with the air temperature (R>0.75). The 18.7, 23.8 and the 36.5 GHz TBs have a low correlation with $T_{Snow-Ice}$ because of microwave scattering in the snow or shallow microwave penetration into the snow. The 7.3 GHz channel is ignored because it contains practically the same information as the 6.9 GHz channel. The TBs at 6.9 and 10.65 GHz in vertical polarization, have the highest correlation with $T_{Snow-Ice}$ (R>0.5). Therefore the 10.65 and the 6.9 GHz in vertical polarization (10V and 6V) channels are selected as inputs to the linear regression to retrieve the $T_{Snow-Ice}$.

4.3 Linear regressions to retrieve the snow-ice interface temperature

To express the $T_{Snow-Ice}$ as a function of the TB at 6V and 10V, the linear regressions are calculated on centered data. For each buoy, the averaged $T_{Snow-Ice}$ is subtracted from the $T_{Snow-Ice}$ measurements (the same is done with the TB measurements). Thus, the temperature offset between the buoys is removed and the slope in the linear regression is unchanged. Figure 6 shows the linear regression between the $T_{Snow-Ice}$ and the TB at 6V and 10V, using the measurements from buoys 2012G, 2012H, 2012J, and 2012L. The slope coefficients estimated between the $T_{Snow-Ice}$ and the TB at 6V and 10V are 1.086±0.020 and 1.078±0.019 respectively.

The offset in the linear regression equations between $T_{Snow-Ice}$ and the TB is different for each buoy, because it depends on the snow depth. The $T_{Snow-Ice}$ dependence on snow depth can be explained by the thermal insulation of snow (Maaß et al.,

The Cryosphere Discuss., https://doi.org/10.5194/tc-2018-223
Manuscript under review for journal The Cryosphere
Discussion started: 12 November 2018

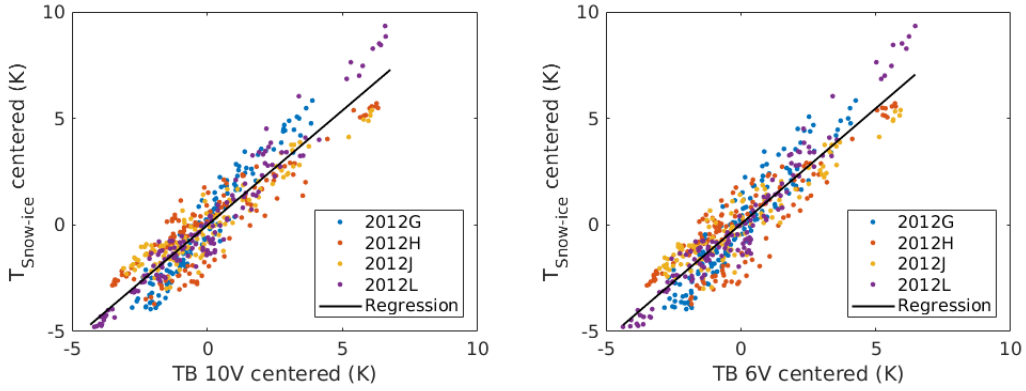

Figure 6. Centered $T_{Snow-Ice}$ expressed as a function of the centered TBs at 10V (left) and 6V (right). Data from the IMB buoys are in colored points and the linear regression is the solid black line.

2013). Here, we establish an empirical relationship between the $T_{Snow-Ice}$ corrected of the TB linear dependence at 10V or 6V, and the snow depth as follows:

$$T_{Snow-Ice} - a_1 \cdot TB_{10V\ or\ 6V} = a_2 \cdot f(SD) + a_3, \tag{2}$$

with $f(SD)$ a function of snow depth.

Three different linear regressions have been tested to relate the $T_{Snow-Ice}$ using: the snow depth directly, the inverse of the snow depth, and the logarithm of snow depth. Figure 7 shows the $T_{Snow-Ice}$ corrected from TB dependence as a function of snow depth. The different regressions are tested using the training dataset (IMB buoys: G, H, J, and L in 2012). The regression showing the best results is the one using the logarithm of the snow depth (solid black line in Fig. 7). The linear regression using the snow depth directly (red dashed line in Fig. 7) leads to an overestimation of the $T_{Snow-Ice}$ for large snow depth. The regression using the inverse of the snow depth (red dotted line in Fig. 7) leads to an underestimation for small snow depth. The RMSEs obtained on the $T_{Snow-Ice}$ are compared and the relation using the logarithm of snow depth shows the lowest RMSE. Based on these results, the final equations to relate the $T_{Snow-Ice}$ to the snow depth and the TB at 10V and at 6V are:

$$T_{Snow-Ice} = 1.078 \cdot TB_{10V} + 5.67 \cdot log(SD) - 5.13 \tag{3}$$

$$T_{Snow-Ice} = 1.086 \cdot TB_{6V} + 3.98 \cdot log(SD) - 10.70 \tag{4}$$

where $T_{Snow-Ice}$ and TB are expressed in K, and SD is expressed in m.

4.4 Results of the snow-ice interface temperature retrieval

Figure 8 shows the comparisons between the observed $T_{Snow-Ice}$ and the regressed $T_{Snow-Ice}$ using the 10V and 6V TBs (Eq. 3 and 4), and the *in situ* snow depth measured by the acoustic sounder of IMB buoys. The regression of the $T_{Snow-Ice}$

The Cryosphere Discuss., https://doi.org/10.5194/tc-2018-223
Manuscript under review for journal The Cryosphere
Discussion started: 12 November 2018

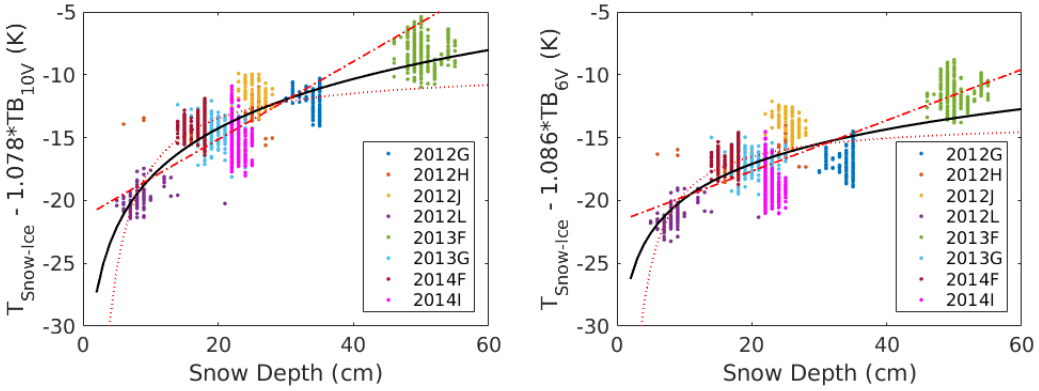

Figure 7. $T_{Snow-Ice}$ corrected of the 10V TB (left) and of the 6V TB (right) dependence as a function of snow depth. Data from the IMB buoys are represented by different colors, the regression using the snow depth is the dashed red line, the regression using the inverse of snow depth is the red dotted line, and the regression using the logarithm of the snow depth is the solid black line.

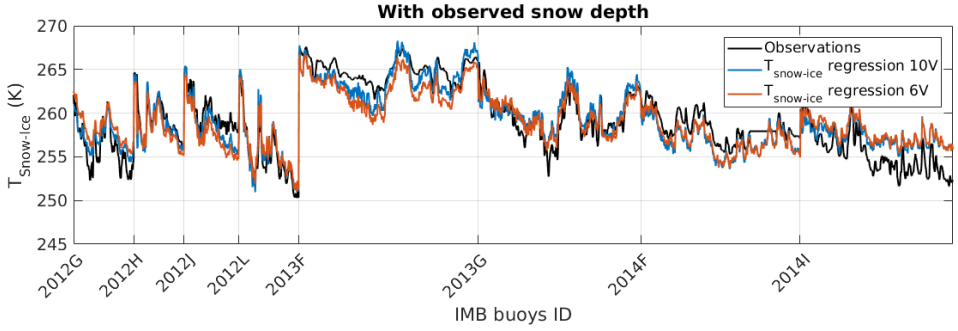

Figure 8. Time series of the comparisons between $T_{Snow-Ice}$ observations from IMB buoys (black line), and $T_{Snow-Ice}$ regressions with TBs at 10V (blue line) and at 6V (red line). The snow depth used in equations 3 and 4 is the snow depth observed by the IMB buoy sounder. The begin of the measurements with a new IMB buoy is indicated on the x-axis.

using the *in situ* snow depth with the 10V TBs (Eq. 3) is slightly better (RMSE = 1.69 K) than the regression with the 6V TBs (Eq. 4) (RMSE = 1.95 K). The variability due to the snow depth is better described with the regression using the 10V TBs. Figure 9 is the same as Figure 8 but using our snow depth estimation (Eq. 1). The RMSEs are 2.78 K for the 10V regression and 2.84 K for the 6V regression. The results are degraded because of the snow depth regression especially for the buoys with thick snow (∼50 cm) or thin snow (∼5 cm) (e.g., buoy 2013F and buoy 2012L). Note that uncertainties can be introduced in the estimate when choosing the level of the snow-ice interface because the vertical resolution of the IMB buoy thermistor string is 10 cm.

The Cryosphere Discuss., https://doi.org/10.5194/tc-2018-223
Manuscript under review for journal The Cryosphere
Discussion started: 12 November 2018

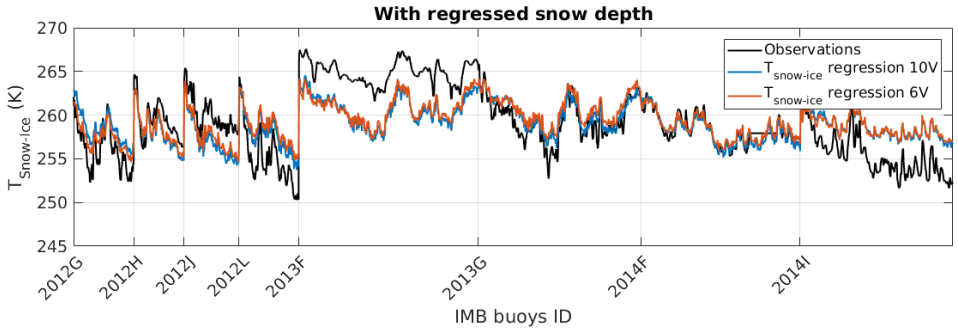

Figure 9. Same as Figure 8, using the regressed snow depth (Eq. 1) in place of in situ snow depth

5 Sea ice effective temperature estimation

5.1 Bias between the model and the observations

The T_{eff} is only available in a simulated dataset using a thermodynamical model and MEMLS. The model set-up and the simulations are described in Tonboe (2010). In this dataset the TBs, the $T_{Snow-Ice}$, and the T_{effs} are simulated together using the input snow and ice profiles from the thermodynamical model. Even though the simulated data are comparable to observations in terms of mean and standard deviation, both the thermodynamical model and the emission model are physical models and they are not tuned to observations. This means that a bias is expected between the $T_{Snow-Ice}$ from MEMLS and the $T_{Snow-Ice}$ from our regressions based on *in situ* observations.

The bias obtained is the mean value of the difference between the $T_{Snow-Ice}$ from MEMLS, and the $T_{Snow-Ice}$ regressed from equations 3 and 4 using the inputs of the simulated data. Biases of 3.97 K and 4.01 K are estimated, for the regressions with 10V and 6V respectively. The RMSEs computed between the $T_{Snow-Ice}$ from MEMLS and the $T_{Snow-Ice}$ regressed and corrected of the bias at 10V and 6V are 2.7 K and 2.07 K, respectively.

Figure 10 shows the $T_{Snow-Ice}$ from MEMLS data as a function of TB at 10V and 6V with the $T_{Snow-Ice}$ computed from our regressions (Eq. 3 and 4), with and without the bias correction. We can see that the slopes of our linear regressions are consistent with the data simulated from MEMLS.

5.2 Linear regression between the effective temperature and the snow-ice interface temperature

The T_{eff} near 50 GHz in vertical polarization is correlated with the $T_{Snow-Ice}$ (Tonboe et al., 2011) and it can be expressed as a linear function of the $T_{Snow-Ice}$. We use the MEMLS simulated data to calculate the linear regression between the $T_{Snow-Ice}$ and the T_{eff} at 6.9, 10.65, 18.7, 23.8, 36.5, 50, and 89 GHz in vertical polarization. T_{effs} at vertical and horizontal polarizations are about the same. Only the vertical polarization is considered here, because TBs measurements are noisier at horizontal polarization due to the variability of sea ice emissivity at this polarization.

The Cryosphere Discuss., https://doi.org/10.5194/tc-2018-223
Manuscript under review for journal The Cryosphere
Discussion started: 12 November 2018

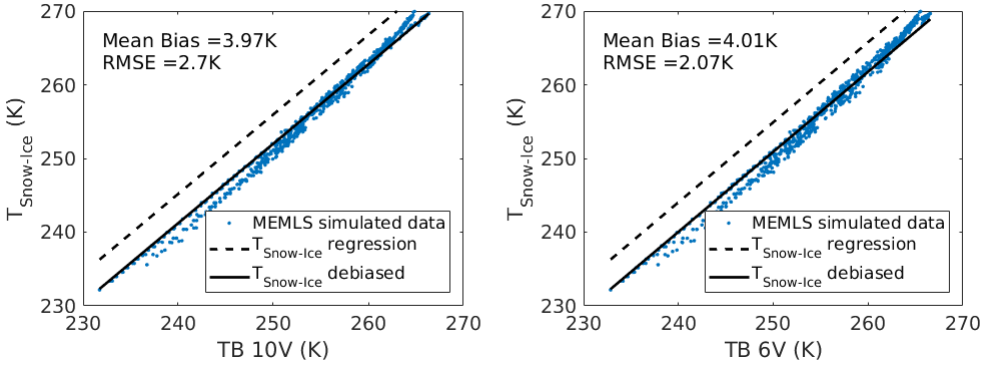

Figure 10. Comparisons between the $T_{Snow-Ice}$ from the MEMLS simulated data in blue points, the regressed $T_{Snow-Ice}$ (Eq. 3 and 4) in dashed black line and the regressed $T_{Snow-Ice}$ debiased to fit the MEMLS simulations in solid black line at 10V (left) and 6V (right) channels.

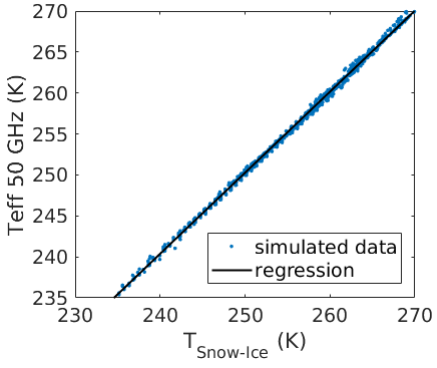

Figure 11. Regression of the $T_{Snow-Ice}$ as a function of T_{eff} at different frequencies. The data from the MEMLS simulations are in blue points and the linear regression is the solid black line.

Figure 11 shows the T_{eff} at 50V as a function of $T_{Snow-Ice}$. The linear regressions between the $T_{Snow-Ice}$ and the T_{eff} at different frequencies are computed. The results are given in Table 3. The slope coefficient of the regression increases with frequency, meaning that the sensitivity of the T_{eff} to the $T_{Snow-Ice}$ is increasing with frequency between 6 and 89 GHz. A slope coefficient lower than 1 means that the emitting layer of the T_{eff} at the given frequency is deeper than snow-ice interface. At 50 GHz the slope coefficient is near to 1, meaning that the emitting layer is at the same depth as the snow-ice interface. The RMSEs obtained are below 1 K, with the regression of T_{eff} at 50V showing the lowest RMSE (0.33 K), and at 89V showing the highest RMSE (0.92 K). These linear regressions between the T_{eff} and the $T_{Snow-Ice}$ are the final step to retrieve the T_{eff} of sea ice at microwave frequencies as a function of TBs, by using the work in the previous section to express the $T_{Snow-Ice}$ as a function of TBs.

The Cryosphere Discuss., https://doi.org/10.5194/tc-2018-223
Manuscript under review for journal The Cryosphere
Discussion started: 12 November 2018

Table 3. Regressions of the T_{eff} for different frequencies at vertical polarization as a function of the $T_{Snow-Ice}$.

Frequency (GHz)	slope coefficient	offset (K)	RMSE (K)
6.9	0.888	30.2	0.89
10.7	0.901	26.6	0.75
18.7	0.920	21.5	0.63
23.8	0.932	18.4	0.57
36.5	0.960	10.9	0.41
50	0.989	2.96	0.33
89	1.06	-16.4	0.92

6 Discussion

For days in November, January, and April, Figure 12 shows the maps of the snow depth estimated with our multilinear regression (Eq. 1), the $T_{Snow-Ice}$ estimated with our multilinear regression (Eq. 3), and the multiyear ice concentration products from the University of Bremen (https://seaice.uni-bremen.de). To perform our regressions, we use the AMSR2 TBs (Level L1R) provided by JAXA and the SIC from the European Centre for Medium-Range Weather Forecasts (ECMWF) Re-Analysis Interim (ERA-Interim) data. Only the areas with 100% SIC are considered to compute the snow depth on sea ice and the $T_{Snow-Ice}$ with our method. Maps of the multiyear ice concentration from University of Bremen are derived from AMSR2 and from the Advanced SCATterometer (ASCAT) with the method of Ye et al. (2016a, b).

The results show that the snow depth is larger (40 cm) in the north of Greenland (Warren et al., 1999) due to the presence of drift snow caused by the numerous pressure ridges present in this area (Hanson, 1980), as anticipated. We can observe that the snow depth is higher in November and April than in January as expected as the snow accumulates moderately during November, very slowly during December and January, and starts to re-accumulate moderately from February to May (Warren et al., 1999).

For $T_{Snow-Ice}$, in January and April when the air temperature is cold ($\sim$ -30° for our situations on January 5 and April 5, 2016), the areas with large snow depth show larger $T_{Snow-Ice}$ because of the thermal insulation power of the snow. It is different in November: the air temperature is warmer ($\sim$ -5°, for the situation on November 5, 2015) and the areas with thinner snow show larger $T_{Snow-Ice}$ which are close to the air temperature. Note that we can observe low $T_{Snow-Ice}$ in some locations near the sea ice margins due to the presence of open ocean in the satellite footprint. As the brightness temperature of open water is low, the total brightness temperature measured is decreased and it impacts our $T_{Snow-Ice}$ estimation.

The Cryosphere Discuss., https://doi.org/10.5194/tc-2018-223
Manuscript under review for journal The Cryosphere
Discussion started: 12 November 2018

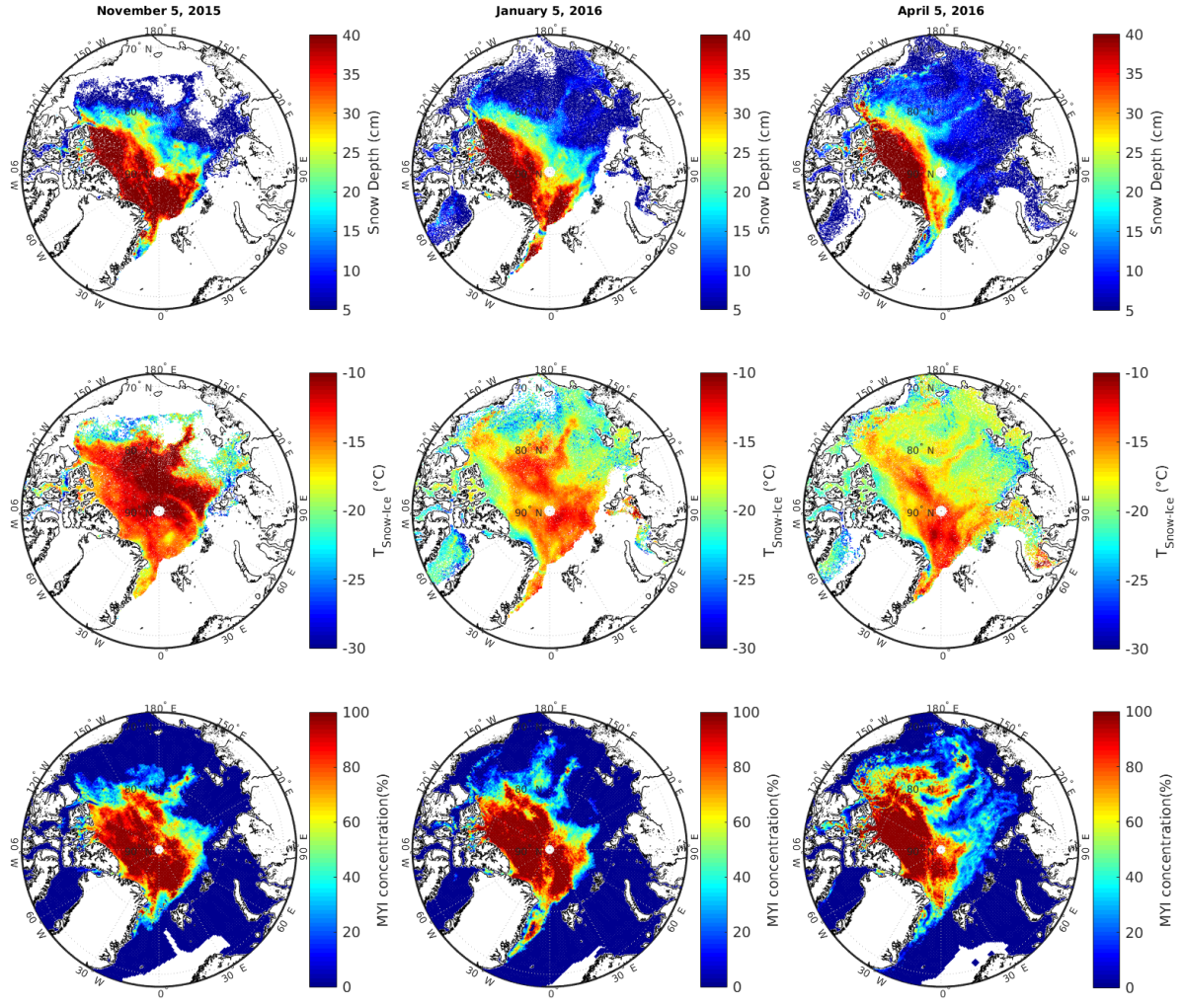

Figure 12. Maps of the snow depth (first row) and the $T_{Snow-Ice}$ (second row) estimated from our multilinear regression using AMSR2 TBs, with MultiYear Ice (MYI) concentration products (third row) from the University of Bremen on November 5, 2015 (left), January 5, 2016 (middle) and April 5, 2016 (right).

Visually the $T_{Snow-Ice}$ shows a high correlation with the distribution patterns of multiyear ice concentration of the same days: the highest values are found in the north of Greenland and in the Canada Basin, with some branches of higher values extending from there towards the Siberian coast, marking the Beaufort gyre of the Arctic sea ice drift (see e.g. the animations for the same year at https://seaice.uni-bremen.de/multiyear-ice-concentration/animations/). The main differences between first-year ice and multiyear ice are, on average, the higher thickness of multiyear ice and its higher snow load . Both effects will influence the $T_{Snow-Ice}$. Under the same conditions, a higher ice thickness will lead to a lower $T_{Snow-Ice}$. In contrast, it will

be higher if only the snow depth is increased. The positive correlation between multiyear ice concentration and $T_{Snow-Ice}$ suggests that the influence of the higher snow depth on multiyear ice outbalances that of the higher ice thickness on the $T_{Snow-Ice}$, emphasizing the important role of snow on sea ice in its thermodynamic balance.

The similar patterns observed between the maps of the $T_{Snow-Ice}$ and the multiyear ice concentration on Figure 12 are encouraging and gives confidence to the methodology developped here, as these multiyear ice concentration products are issued from a completely independent estimation done at the University of Bremen and distributed daily to users.

7 Conclusions

We derive simple algorithms to estimate sea ice parameters such as the snow depth, the $T_{Snow-Ice}$, and the T_{eff} of sea ice at microwave frequencies, from AMSR2 channels. This is achieved using the ESA RRDP which contains AMSR2 data collocated with IMB buoy data and OIB campaign data. In addition, simulated TB output from a sea ice version of MEMLS are used for the regression of the T_{eff}. All the equations to retrieve these sea ice parameters are derived using several linear and multilinear regressions.

Our regression to retrieve the snow depth over winter Arctic sea ice uses the TBs at 6.9, 18.7 and 36.5 GHz in vertical polarization. A RMSE of 6 cm is obtained on the estimated snow depth. To retrieve the $T_{Snow-Ice}$, two relations are derived using two different AMSR2 channels: 10V and 6V, and the snow depth. The two regressions show similar results. The errors obtained are 1.69 K and 1.95 K respectively at 10V and 6V. Finally the T_{effs} at 6.9, 10.65, 18.7, 23.8, 36.5, 50, and 89 GHz in vertical polarization are retrieved as a function of $T_{Snow-Ice}$ using linear regressions. At the final step, the RMSEs of the linear regressions between the simulated $T_{Snow-Ice}$ and the T_{eff} for all channels are lower than 1 K, with a minimum value of 0.33 K at 50 GHz which is a key frequency for atmosphere temperature retrieval. The methodology to estimate snow depth and $T_{Snow-Ice}$ has been applied to several days during a winter season. It shows consistent results with multiyear ice concentration estimates obtained independently.

These algorithms can be used to create snow depth and $T_{Snow-Ice}$ products which can improve the study of sea ice variability (e.g., sea ice growth). Informations on the $T_{Snow-Ice}$ may help in sea ice models by constraining the sea ice temperature gradient and the thermodynamical ice growth. The T_{eff} estimations can be used in atmospheric radiative transfer calculations and to reduce noise in SIC retrieval algorithms (Tonboe et al., 2013) (e.g., EUMETSAT OSISAF global SIC product).

Author contributions. This study was conducted by L.K. and supervised by R.T.T. and C.P.. G.H. contributed to the analysis and to the correction of the draft.

Competing interests. The authors declare no conflict of interest.

Acknowledgements. This research was funded by EUMETSAT OSISAF (OSI VS17 03). The authors acknowledge the support from the EUMETSAT OSISAF visiting scientist program and the Danish Meteorological Institute for its welcome.

References

Comiso, J., Cavalieri, D., and Markus, T.: Sea ice concentration, ice temperature, and snow depth using AMSR-E data, IEEE Trans. Geosci. Remote Sens., 41, 243–252, 2003.

Dybkjær, G., Tonboe, R., and Høyer, J. L.: Arctic surface temperatures from Metop AVHRR compared to in situ ocean and land data, Ocean Sci., 8, 959–970, 2012.

English, S. J.: The Importance of Accurate Skin Temperature in Assimilating Radiances From Satellite Sounding Instruments, IEEE Trans. Geosci. Remote Sens., 46, 403–408, 2008.

Grönfeldt, I.: Snow and sea ice temperature profiles from satellite data and ice mass balance buoys, Tech. rep., Lund University, 2015.

Hanson, A. M.: The Snow Cover of Sea Ice during the Arctic Ice Dynamics Joint Experiment, 1975 to 1976, Arctic and Alpine Research, 12, 215–226, https://doi.org/10.1080/00040851.1980.12004180, 1980.

Harlow, R.: Millimeter Microwave Emissivities and Effective Temperatures of Snow-Covered Surfaces: Evidence for Lambertian Surface Scattering, IEEE Trans. Geosci. Remote Sens., 47, 1957–1970, 2009.

Harlow, R. C.: Sea Ice Emissivities and Effective Temperatures at MHS Frequencies: An Analysis of Airborne Microwave Data Measured During Two Arctic Campaigns, IEEE Trans. Geosci. Remote Sens., 49, 1223–1237, 2011.

Lecomte, O., Fichefet, T., Vancoppenolle, M., and Nicolaus, M.: A new snow thermodynamic scheme for large-scale sea-ice models, Annals of Glaciology, 52, 337–346, https://doi.org/10.3189/172756411795931453, 2011.

Lindsay, R. W., Rothrock, D. A., Lindsay, R. W., and Rothrock, D. A.: Arctic Sea Ice Surface Temperature from AVHRR, J. Clim., 7, 174–183, 1994.

Maaß, N., Kaleschke, L., Tian-Kunze, X., and Drusch, M.: Snow thickness retrieval over thick Arctic sea ice using SMOS satellite data, The Cryosphere, 7, 1971–1989, https://doi.org/10.5194/tc-7-1971-2013, 2013.

Markus, T. and Cavalieri, D. J.: Snow Depth Distribution Over Sea Ice in the Southern Ocean from Satellite Passive Microwave Data in Antarctic Sea Ice: Physical Processes, Interactions and Variability (ed M. O. Jeffries), pp. 19–39, American Geophysical Union, Washington, D. C, 1998.

Mathew, N., Heygster, G., Melsheimer, C., and Kaleschke, L.: Surface Emissivity of Arctic Sea Ice at AMSU Window Frequencies, IEEE Trans. Geosci. Remote Sens., 46, 2298–2306, 2008.

Mätzler, C.: Thermal microwave radiation : applications for remote sensing, Institution of Engineering and Technology, London, United Kingdom, 2006.

Maykut, G. A. and Untersteiner, N.: Some results from a time-dependent thermodynamic model of sea ice, Journal of Geophysical Research, 76, 1550–1575, https://doi.org/10.1029/JC076i006p01550, 1971.

Pedersen, L. F. and Saldo, R.: Sea Ice Concentration (SIC) Round Robin Data Package , Sea Ice Climate Initiative: Phase 2, Tech. Rep. SICCI-RRDP-07-16 Version: 1.4, ESA, 2016.

Perovich, D. K., Richter-Menge, J. A., Elder, B., Claffey, K., and Polashenski, C.: Observing and understanding climate change: monitoring the mass balance, motion, and thickness of Arctic sea ice, Tech. rep., Cold Regions Research and Engineering Laboratory., 2017.

Rosenkranz, P. W. and Mätzler, C.: Dependence of AMSU-A Brightness Temperatures on Scattering From Antarctic Firn and Correlation With Polarization of SSM/I Data, IEEE Geosci. Remote Sens. Lett., 5, 769–773, 2008.

Sato, K. and Inoue, J.: Comparison of Arctic sea ice thickness and snow depth estimates from CFSR with in situ observations, Climate Dynamics, 50, 289–301, 2018.

Tonboe, R. T.: The simulated sea ice thermal microwave emission at window and sounding frequencies, Tellus A: Dynamic Meteorology and Oceanography, 62, 333–344, 2010.

Tonboe, R. T., Dybkjær, G., and Høyer, J. L.: Simulations of the snow covered sea ice surface temperature and microwave effective temperature, Tellus A Dyn. Meteorol. Oceanogr., 63, 1028–1037, 2011.

Tonboe, R. T., Schyberg, H., Nielsen, E., Rune Larsen, K., and Tveter, F. T.: The EUMETSAT OSI SAF near 50 GHz sea ice emissivity model, Tellus A Dyn. Meteorol. Oceanogr., 65, 18 380, 2013.

Wang, D., Prigent, C., Kilic, L., Fox, S., Harlow, C., Jimenez, C., Aires, F., Grassotti, C., and Karbou, F.: Surface Emissivity at Microwaves to Millimeter Waves over Polar Regions: Parameterization and Evaluation with Aircraft Experiments, Journal of Atmospheric and Oceanic Technology, 34, 1039–1059, https://doi.org/10.1175/JTECH-D-16-0188.1, 2017.

Warren, S. G., Rigor, I. G., Untersteiner, N., Radionov, V. F., Bryazgin, N. N., Aleksandrov, Y. I., and Colony, R.: Snow Depth on Arctic Sea Ice, Journal of Climate, 12, 1814–1829, 1999.

Wiesmann, A. and Mätzler, C.: Microwave Emission Model of Layered Snowpacks, Remote Sens. Environ., 70, 307–316, 1999.

Ye, Y., Heygster, G., and Shokr, M.: Improving Multiyear Ice Concentration Estimates With Reanalysis Air Temperatures., IEEE Trans. Geoscience and Remote Sensing, 54, 2602–2614, 2016a.

Ye, Y., Shokr, M., Heygster, G., and Spreen, G.: Improving multiyear sea ice concentration estimates with sea ice drift, Remote Sensing, 8, 397, 2016b.